

Development of a Novel Mixed Titanium, Silver Oxide Polyacrylonitrile Nanofiber as a Superior Adsorbent and its Application for MB Removal in Wastewater Treatment

Zhiqun Xu,^a Congcong Wei,^a Jiali Jin,^a Wenkai Xu,^b Qiao Wu,^a Junjie Gu,^a Minrui Ou^a
and Xiaoping Xu^{*a}

^aKey Laboratory of Biopharmaceutical, College of Chemistry and ^bCollege of Civil Engineering,
Fuzhou University, 350108 Fuzhou, P. R. China

In this study, a novel electrospun nanofibrous composite was synthesized from polyacrylonitrile (PAN) and well-dispersed oxide nanoparticles containing Ti and Ag (PAN-TA). The nanoparticles incorporated into the nanofibers can endow the composite with photocatalytic and antimicrobial ability. The morphologies and structure of the nanofibers were characterized by Fourier transform infrared (FTIR), scanning electron microscopy (SEM) and X-ray diffraction (XRD). Controlled experiments were carried out with the effects of chemical modification, solution pH, temperature, dosage, contact time, and initial concentration of the dye. The methylene blue (MB) dye was completely removed within 20 min at room temperature 25 °C with high maximum retention capacity of 155.4 mg g⁻¹. Moreover, equilibrium data and kinetics data indicated that the dye adsorption agreed well with the Langmuir isotherm model and pseudo-second order model, respectively. In addition, the nanofibers could be easily separated from dye solution and showed high reusability for numerous repeat cycles, thus indicating good application prospects for the wastewater treatment.

Keywords: adsorption, methylene blue, polyacrylonitrile, nanoparticles

Introduction

Industrial wastewaters have been considered as one of the largest sources of water pollution.^{1,2} Organic dyes are common in effluents discharged by various industries such as textile, paper, leather and printing industries.^{3,4} According to some statistics, approximately 70,000 metric tons of commercial dyes are discharged into wastewater each year all over the world.⁵ Furthermore, many dyes and their incomplete degradation products have complex constitution, fluctuating water quality, high chemical oxygen demand (COD) level, deep and long-lasting color, and high toxicity, which is a nuisance to the aquatic biosphere.⁶ Methylene blue (MB) is a kind of cationic dye with broad applications. It has been used in many fields such as colorants for paper, strainers for medicinal surgery, and hair and cotton, among others.⁷ However, it will also result in disease like retching, stun, cyanosis, jaundice, and tissue necrosis in humans.^{8,9} As a result, the removal of dyes from industrial wastewaters has become environmentally critical.

To date, many strategies including chemical oxidation,¹⁰ membrane filtration,¹¹ adsorption¹² and photocatalysis¹³ have been developed to reduce the pollution and hazards of MB. Among various approaches towards MB removal from wastewater, adsorption and photocatalysis have been found to be superior to other methods because of its attractive features such as economical and effective method with a simple process.¹⁴ Many adsorbents are introduced such as activated carbon,¹⁵ sawdust,¹⁶ perlite,¹⁷ soybean hull,¹⁸ kaolinite clay,¹⁹ and rice straw.²⁰ However, they suffer from some limitations such as mechanical resistance, poor heat, and low adsorption capacity.²¹ A good adsorbent should generally possess a porous structure, and the time required for adsorption equilibrium should be as small as possible.²²

Polyacrylonitrile (PAN) is known as a common and environmentally stable commercial polymer, with desirable chemical, thermal properties and good solubility in organic solvents.^{23,24} This polymer has been widely used in the production of nanofibers via electrospinning process.²⁵ Recently, PAN surface modification has been performed by many researchers using diethylenetriamine, polyethyleneimine and ethylenediamine for heavy metal ions and dye adsorption.²⁶ It is reported that mixed metal

*e-mail: xu@fzu.edu.cn

oxides containing two or more metals were effective catalysts and catalytic supports for a wide variety of organic reactions.^{27,28} Taking advantage of the high specific surface area of nanostructures, TiO₂ and other metal oxides have been utilized to enhance dye degradation adsorption purpose.^{29,30}

For example, Zhou *et al.*³¹ successfully prepared a nano-TiO₂/chitosan/poly(*N*-isopropylacrylamide) (nano-TiO₂/CS/PNIPAAm) composite hydrogel. The hydrogel exhibited high efficiency of photocatalytic degradation for Alexa fluor (AF) dyes and removal efficiency of AF dye reached 90.5% under UV irradiation for 160 min. Pal *et al.*³² synthesized mixed oxide nanoparticles containing titanium, aluminum and/or silicon in different proportions through a combined sol-gel-hydrothermal method and explored their cationic dye adsorption behavior. It has been shown that the addition of aluminum and/or silicon in titania nanoparticles (NPs) improves their cationic dye adsorption capacity significantly.

In this work, PAN-based nanofibers were prepared by combining the electrospinning technique and the chemical modification of nitrile group in PAN copolymer containing titanium and silver in different proportions. The dye removal efficiency and adsorption capacity of the adsorbent were studied using the UV-Vis spectrometer. The prepared PAN-TiO₂-Ag₃VO₄ (PAN-TA) nanofibers were proved as a high-performance adsorbent toward MB removal. Adsorption and regeneration were performed efficiently up to 6 cycles. To the best of our knowledge, this is the first report on the use of electrospinning PAN-TA nanofibers for removal of dye pollutants.

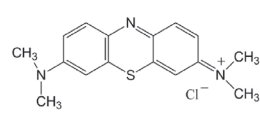
Experimental

Chemicals and reagents

All chemical reagents and solvents used in this experiment were reagent grade or better and used without further purification unless otherwise stated. Deionized (DI) water was used throughout all experiments (prepared by Fuzhou University, Fuzhou, China). Polyacrylonitrile (PAN, Mw = 150000), TiO₂ agglomerates (P25, Degussa particle size 21 nm), silver nitrate (AgNO₃), sodium vanadate (Na₃VO₄) and methylene blue were purchased from Sigma (St. Louis, USA). The *N,N*-dimethyl formamide (DMF), hydrochloric acid (HCl), methanol and sodium hydroxide (NaOH) used were purchased from Aladdin (Shanghai, China). DI water was used to prepare all the dye solutions. The chemical structure of the dye was shown in Figure 1.

Measurements

UV-Vis absorption spectra were recorded on a



Property	Value
Molecular formula	C ₁₆ H ₁₈ N ₃ ClS
CAS	61-73-4
Molecular weight	319.858
EINECS	200-515-2
Water solubility (20 °C) / (g L ⁻¹)	40
λ _{max} / nm	664

Figure 1. Characteristics of methylene blue.

U-4100 spectrophotometer. FTIR spectra were recorded using a JASCO FTIR 620 spectrometer in the range of 4000-400 cm⁻¹. The scanning electron microscopy with energy-dispersive X-ray spectroscopy (SEM-EDS) analysis was performed using field emission scanning electron microscope (FE-SEM; S-4700, Hitachi, Tokyo, Japan) equipped with energy dispersive X-ray spectroscopy (EDS). The crystalline structure of nanofiber was characterized by the X-ray diffraction (XRD) technique on Rigaku Ultima IV (Japan) by employing Cu-Kα radiation (λ = 1.5406 Å) with visible light at 45 kV and 40 mA. All pH measurements were made with a Model PHS-3C meter.

Sample preparation

To be brief, a solution of 10% (m/m) polyacrylonitrile in DMF was prepared by constant mechanical stirring under the water bath condition at 50 °C for about 24 h. Then a solution containing silver nitrate (100 mg, based on polymer solution) was prepared. Sequentially, various amounts of TiO₂ (0.05, 0.1 and 0.15 g) NPs were dispersed in the polymer solution and the TiO₂ NPs solution was sonicated for 12 h.

For the electrospinning process, the as-prepared solutions were then electrospun under a fixed electric field of 15 kV, using a gamma high voltage research RR60 power supply. A piece of aluminum foil (20 × 20 cm) on the collector was 15 cm from the tip of the needle with the feeding rate of 1.3 mL h⁻¹. A piece of the initial PAN-based nanofibers was immersed in a Na₃VO₄ aqueous solution (0.2 M) at room temperature for the ion exchange reaction. The color of the composite nanofibers turned to yellow in a few minutes, indicating the formation of Ag₃VO₄ NPs on the surface of polymer nanofibers via the reaction of Ag⁺ with VO₄³⁻. Then, it was washed with DI water and immersed into a 100 mL of 0.1 g g⁻¹ NaOH aqueous solution for 1 h at 50 °C before being placed in 1 mol L⁻¹ HCl aqueous solution at room temperature for 3 h. After this step, the obtained nanofibers were taken out and washed thoroughly with DI to remove the impurities. It should be completely dried in vacuum drier at 50 °C before using. The corresponding procedures (synthesis and modification of PAN-based nanofibers) are described visually in Figure 2.

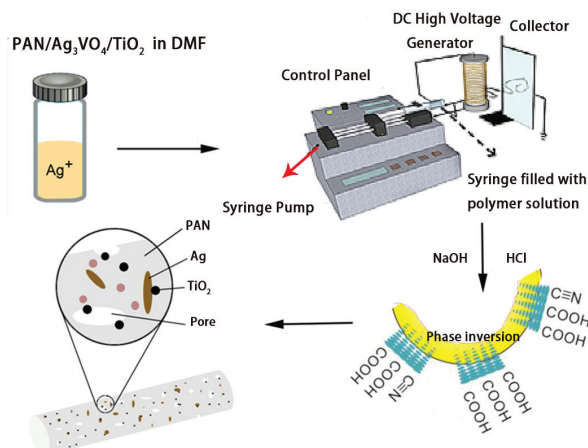


Figure 2. Fabrication of PAN-TA composite nanofibers.

Adsorption tests

A batch method was used to perform MB sorption experiments. Stock solution of 1000 mg L⁻¹ of MB was prepared in DI water. The pH of the solution was adjusted using HCl or NaOH (1 M). Adsorption studies were completed utilizing weighed modified nanofibers as a superior adsorbent in a temperature controlled incubator shaker (150 rpm, 20 °C, 10 h in 100 mL glass bottles). Water samples were collected at a depth of 2 cm in the upper phase and the absorbance of the supernatant was recorded at 664 nm. Calibration curves were plotted between the absorbance and the concentration of the MB dye solution. All the adsorption experiments were performed three times and the mean taken to eradicate any discrepancies. Adsorption capacity (q_e) and removal efficiency (R) were calculated using following equations:

$$R = \left(\frac{C_0 - C_e}{C_0} \right) \times 100\% \quad (1)$$

$$q_e = \frac{(C_0 - C_e)V}{m} \quad (2)$$

where q_e is adsorption capacity (mg g⁻¹), C_0 and C_e are initial and equilibrium concentration of dye (mg L⁻¹), respectively, m is the amount of adsorbent used (g) and V is the volume of solution (L).

Antimicrobial test

In order to test antimicrobial activities of the as-spun nanofibers, Gram-negative *Escherichia coli* (*E. coli*) bacteria was selected as the target and the modified Kirby-Bauer method was used.³³ *E. coli* was cultivated in sterilized tryptic soy broth and incubated overnight at 37 °C in a shaking

incubator. Separately, 100 μL of *E. coli* suspension (OD₆₀₀ around 0.6) was cultured on Luria-Bertani (LB) agar plates. Then, each prepared sample disk with a diameter of 13 mm, which had been sterilized by UV irradiation for 30 min before, was gently placed on the center of the LB agar plates and incubated overnight at 37 °C. Finally, the radius of the inhibition zone was used to evaluate the antimicrobial capability of the PAN-TA nanofibers after 16 h.

Isotherm and kinetic models

Absorption isotherms

The adsorption capacity of adsorbent and interaction mode between adsorbent and adsorbates is another critical factor for the practical use of the adsorbent. The isotherm data for MB adsorption onto PAN-TA was correlated by Langmuir, Freundlich, and Temkin isotherms. The Langmuir model is obtained by assuming that sorbate is homogeneously adsorbed onto an energetically homogenous adsorbent surface, where all the binding sites are identical and with equal adsorption activation energy.³⁴ Langmuir model is expressed by the equation:

$$q_e = \frac{q_L k_L C_e}{1 + k_L C_e} \quad (3)$$

where q_e (mg g⁻¹) is the MB adsorption capacity at equilibrium, C_e (mg L⁻¹) the concentration of adsorbate in the liquid phase at equilibrium, q_L (mg g⁻¹) is the maximum MB adsorption capacity of PAN-TA, and k_L (L mg⁻¹) is the constant related to the rate of adsorption.

Otherwise, the Freundlich model is used to describe the adsorption on heterogeneous surfaces, which is characterized by a heterogeneity factor of $1/n$. This model is a power-type function and it is not restricted to the production of the monolayer.³⁵ Freundlich model is expressed by the equation:

$$q_e = k_f C_e^{1/n} \quad (4)$$

where k_f and $1/n$ indicate the extent and strength of attraction, respectively.

The Temkin isotherm is obtained by assuming that the free energy of adsorption is a function of the surface coverage and takes into account the interactions between adsorbents and adsorbates.³⁶ Temkin model is expressed by the equation:

$$q_e = \beta \ln k_T + \beta \ln C_e \quad (5)$$

where the constant $\beta = RT / b$ (L mg⁻¹) is related to

the heat of adsorption, k_T (mg L^{-1}) is a constant of the Tempkin isotherm and b (J mol^{-1}) is the energy constant, R ($8.314 \text{ J K}^{-1} \text{ mol}^{-1}$) is the gas constant and T (K) is the absolute temperature.

Adsorption kinetic studies

To further understand the mechanism of solute sorption onto adsorbent, we employed kinetic models. Since the adsorbate residence time and reactor dimensions were controlled by the kinetics of the system, it is important to know the rate of adsorption during contaminant removal from wastewater. At this point, three kinetic models were used to analyze and simulate the adsorption data which are: pseudo first-order equation (PFO),³⁷ pseudo-second-order equation (PSO)³⁸ and intra-particle diffusion equation (IPD).³⁹ A linear form of pseudo-first order model is given by the equation:

$$\log(q_e - q_t) = \log q_e - \frac{k_1 t}{2.303} \quad (6)$$

The pseudo-second-order adsorption model can be expressed as follows:

$$\frac{t}{q_t} = \frac{1}{k_2 q_e^2} + \frac{1}{q_e} t \quad (7)$$

where q_e and q_t (mg g^{-1}) are the adsorption capacities at equilibrium and at certain adsorbing time. k_1 and k_2 (L min^{-1}) are the rate constants for each model.

The value of half-adsorption time ($t_{1/2}$) is an important measure of the rate of adsorption, which represents the time required for adsorbent to uptake half of the dye amount at equilibrium. As intra-particle diffusion resistance affects adsorption, it was explored by using the intra-particle diffusion model (IPD) by the equation:

$$q_t = k_p t^{1/2} + I \quad (8)$$

where k_p and I are the intra-particle diffusion rate constant and intercept, respectively.

Desorption and regeneration

In desorption experiments, HCl solution was used as the desorbing agent. 30 mL of the desorbing agents mixed with nanofibers (previous used for absorbing 20 mg mL^{-1} MB) samples and reacted for 2.5 h at 25°C . By using magnetic separation, the sample was then separated from the solution and washed with ultra-pure grade water three times for

another recycle before drying. Each adsorption-desorption experiment was repeated five times. The desorption capacity of the desorbing agent (D , %) is calculated by equation:

$$D(\%) = \frac{C_d}{C_a} \times 100\% \quad (9)$$

where C_d and C_a are the desorbed concentration and adsorbed concentration (mg mL^{-1}), respectively.

Results and Discussion

FTIR characterization

To examine the functional groups present in the electrospun nanofiber composite, the FTIR spectra of untreated PAN, modified PAN-TA and MB-loaded PAN-TA are explored (Figure 3). Untreated PAN spectrum (curve a) exhibited the absorption peaks at 2243 cm^{-1} , which was attributed to the stretching vibration band of nitrile groups ($-\text{CN}$). Two strong adsorption peaks appeared at 2939 and 1454 cm^{-1} and were attributed to the stretching and bending vibration band of methylene ($-\text{CH}_2-$) on the surface. In the spectrum of the NaOH-treated nanofibers (PAN-TA, curve b), there were two prominent peaks in the 3428 and 1692 cm^{-1} region, which was due to the presence of O-H and C=O bonds of carboxylic acids in the surface of the nanofibers. These two stretching peaks indicated that $-\text{COOH}$ is present in the electrospun nanofiber composite after treatment with NaOH and HCl solutions. For the FTIR spectrum of MB-loaded PAN-TA (curve c), two peaks at 3060 and 2927 cm^{-1} represent the stretching vibration of $-\text{CH}$ aromatic and $-\text{CH}_3$ methyl groups of MB. The band near 1488 cm^{-1} is related to the $-\text{CH}_3$ peak and the feature

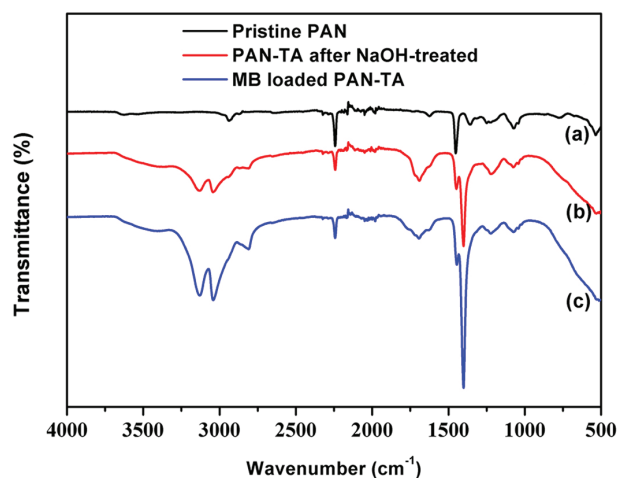


Figure 3. FTIR spectra of PAN (curve a); modified PAN-TA nanofibers (curve b) and MB-loaded PAN-TA nanofibers (curve c, dose = 20 mg L^{-1} , shaking speed = 150 rpm and temperature = 25°C).

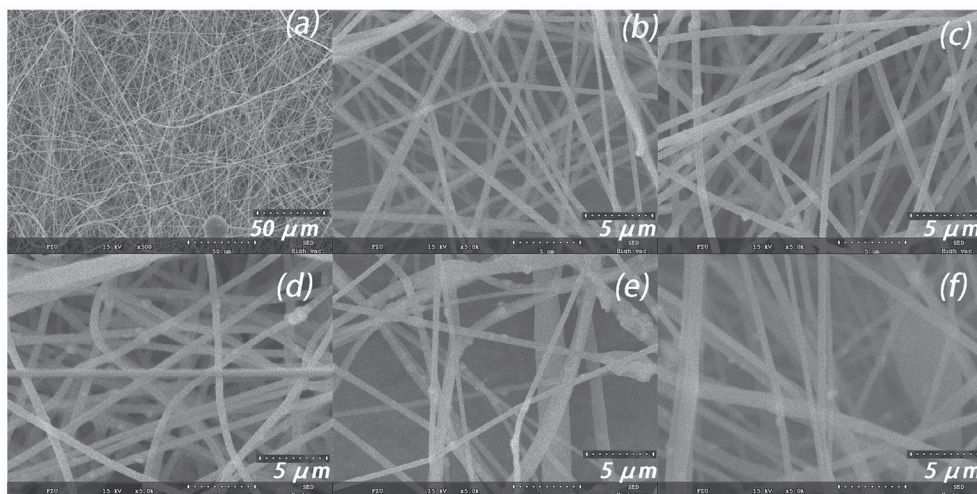


Figure 4. Field-emission scanning electron microscopy images; (a) and (b) pristine PAN nanofibers; (c) PAN + 0.5 wt.% $\text{TiO}_2/\text{Ag}_3\text{VO}_4$; (d) PAN + 1 wt.% $\text{TiO}_2/\text{Ag}_3\text{VO}_4$; (e) PAN + 1.5 wt.% $\text{TiO}_2/\text{Ag}_3\text{VO}_4$; (f) PAN + 1.5 wt.% $\text{TiO}_2/\text{Ag}_3\text{VO}_4$ after MB adsorption.

conforming to the C=C skeleton stretching at 1596 cm^{-1} originates from the aromatic ring vibrations of MB dye. This further confirms the adsorption of MB on to PAN-TA nanofibers.

Morphology of various surface-modified PAN nanofibers

The SEM images of PAN and different PAN-TA nanofibers modified by $\text{TiO}_2/\text{Ag}_3\text{VO}_4$ nanoparticles are presented in Figure 4. A typical raw fiber had a diameter 210 nm with a compact, dense, rough surface (Figure 4a). It can be seen that the surface of all PAN-TA nanofibers became rougher than the untreated PAN nanofiber which reveals that TiO_2 and Ag_3VO_4 nanoparticles were well decorated on the surface of the PAN nanofibers (Figure 4b). In addition, the average diameter of nanofibers increased from 210 nm (for the untreated PAN nanofiber) to 230, 240, and 310 nm for PAN + 0.5 wt.% $\text{TiO}_2/\text{Ag}_3\text{VO}_4$, PAN + 1 wt.% $\text{TiO}_2/\text{Ag}_3\text{VO}_4$, PAN + 1.5 wt.% $\text{TiO}_2/\text{Ag}_3\text{VO}_4$, respectively, which was attributed to the swelling of nanofibers during functionalization. After soaking the PAN-TA nanofibers in MB dye solution, the PAN-TA nanofibers became smooth and compact with few pores. The complex and microspore surface of original PAN-TA was related to the abundance of the binding sites and regions, and they were occupied by MB molecules after adsorption.

XRD characterization

X-ray diffraction patterns of pristine PAN, PAN + 0.5 wt.% TA, PAN + 1.0 wt.% TA, PAN + 1.5 wt.% TA and MB loaded nanofibers are presented in Figure 5. Pattern (a) revealed a broad peak at $2\theta = 16.9^\circ$, a characteristic peak

of PAN nanofibers. This peak is observed for three other samples in lower intensities because of higher attenuation of incident X-ray by high atomic number Ti nuclei and Ag nuclei. The typical diffraction peak at $2\theta = 25^\circ$ assigned to TiO_2 can be observed in these samples, which are in good agreement with the results reported by Ma *et al.*⁴⁰ Moreover, the peaks of PAN are not clearly observed in the pattern of PAN-TA, which is attributed to a lower crystallinity from PAN than metal NPs.

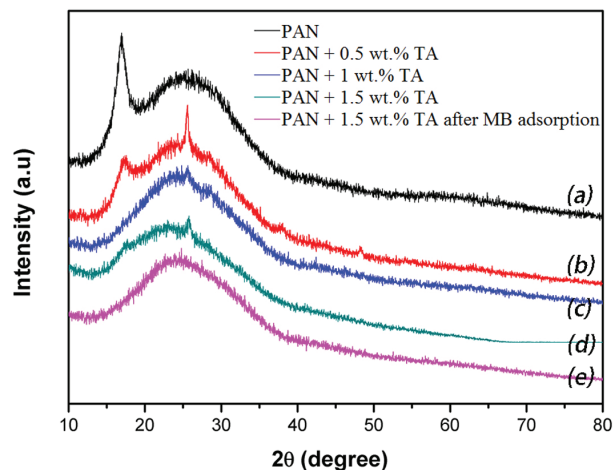


Figure 5. XRD for pristine PAN nanofibers; PAN + 0.5 wt.% TA; PAN + 1.0 wt.% TA; PAN + 1.5 wt.% TA and MB loaded nanofibers.

Adsorption studies

To better investigate the adsorption performance of PAN-TA nanofibers (PAN + 1 wt.% $\text{TiO}_2/\text{Ag}_3\text{VO}_4$) towards MB, different influence factors, such as pH, contact time, temperature, adsorbent dosage, MB concentration, adsorption kinetics and adsorption isotherms about the experiment were conducted.

Effect of pH on adsorption

One of the important factors which could affect the dye adsorption is pH since it influences the charge transfer on the solid/liquid interface.²⁶ Figure 6a demonstrated the

experimental results with a wide pH range. The removal efficiency increased when the solution pH increased from 3.0 to 8.0. With further increase in solution pH, the dye adsorption rate was not significant. A maximum adsorption efficiency approached 95% where the majority of carboxylic

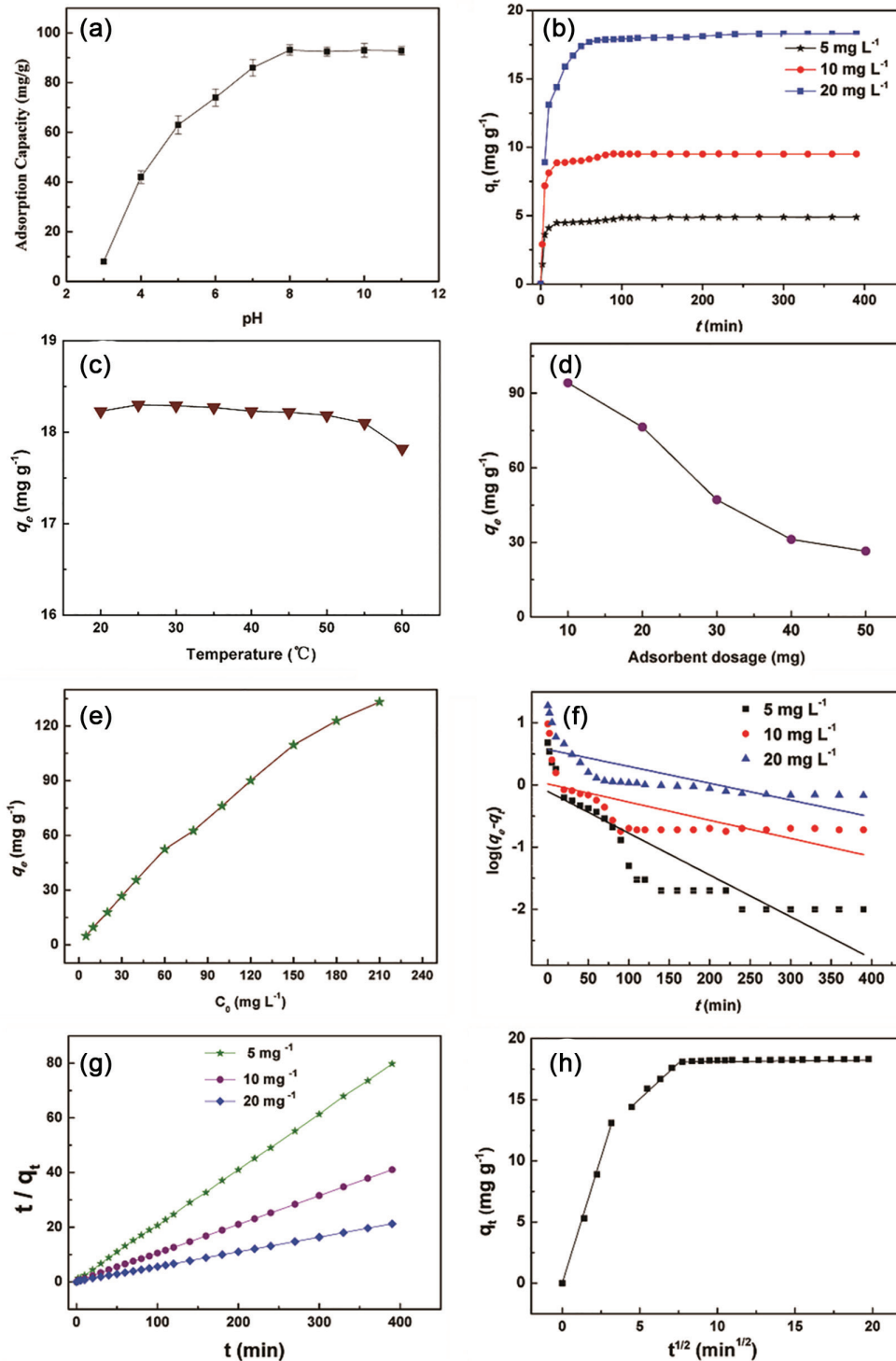


Figure 6. Effect of (a) pH; (b) contact time (C_0 : 5, 10 and 20 mg L^{-1} , 25 $^{\circ}\text{C}$, pH: 8) toward MB adsorption on PAN-TA; (c) temperature (C_0 : 20 mg L^{-1} , 2 h, pH: 8) toward MB adsorption on the PAN-TA; (d) adsorbent dosage; (e) initial dye concentration; (f) pseudo-first order kinetics; (g) pseudo-second order kinetics and (h) intra-particle diffusion (C_0 : 20 mg L^{-1} , 25 $^{\circ}\text{C}$, pH: 8).

groups are ionized upon contact with the dye molecules, which improved the removal efficiency of the cationic MB dye. For the prepared PAN-TA nanofibers, there are massive functional groups in the structure of polymeric network, including nitrile groups and hydroxyl groups. The strong interactions between the electropositive MB molecules and the massive electronegative hydroxyl groups in the polymer chains greatly increased the adsorption efficiency. Besides this, the hydroxyl groups can form hydrogen bonds with amine groups of MB molecules. Moreover, when the dye molecules approach the adsorbent, electrostatic interaction will be the dominant force to attract the dye molecules, which give the adsorbent excellent performance.

Effect of contact time

Effect of contact time on the removal of MB dye by PAN-TA nanofibers was studied with 0.01 g of PAN-TA nanofibers at its initial MB concentration of 5, 10, and 20 mg L⁻¹ at 25 °C. As shown in Figure 6b, MB removal was very rapid at the initial contact time and the adsorption equilibrium reached within 20 min. The initial rapid adsorption is attributed to the availability of the active adsorption sites suitably exposed on surface, as well as interior of PAN-TA which becomes saturated as a function of time. The corresponding calculated removal efficiencies were 97.8, 95.1 and 91.5%, respectively, suggesting its high efficiency for removal of MB.

Effect of temperature

Furthermore, the influence of temperature was also studied (seen in Figure 6c). It was shown that the adsorption capacity of MB increased first and then descended with the increasing temperature, indicating that 25 °C was a proper temperature to remove MB dye. It was also noted that the electrostatic interaction between PAN-TA nanofibers and MB will be weakened if the temperature is too high.

Effect of adsorbent dosage

Five different PAN-TA dosages (10-50 mg) were performed to determine the effect of PAN-TA dosage on the adsorption capacity (Figure 6d). Significant changes in the adsorption capacity among different PAN-TA dosages were observed. The trend shows that with the increase of dosage, the adsorption capacity decrease. Moreover, the lowest dosage of 10 mg shows the highest adsorption capacity. The introduction of active sites on the surface of nanofibers links directly to increasing dye removal. However, the aggregation of adsorption sites will further

result in a decrease in the surface area of the total adsorbent available for the dye molecules and an increase in the length of the diffusion path. This result is consistent with previous reports in the literature.⁴¹

Effect of MB concentration

It was found that adsorption capacities of MB increased with the increase in initial dye concentration from 5 to 210 mg L⁻¹ (Figure 6e). This can be explained by the fact that the higher initial dye concentration, the greater driving force to overcome the mass transfer resistance of dye molecules between the aqueous and solid phases, so higher adsorption capacities were obtained at higher initial dye concentration. However, the percentage removal of MB decreased with increase in initial dye concentration. At a given adsorbent dosage, the limited number of available adsorption sites allowed that only part of dye molecules could be adsorbed. Therefore, the percentage of MB removal was higher at lower initial dye concentration but lower at higher initial dye concentration.

Adsorption kinetics of PAN-TA for MB

To study the adsorption kinetics of PAN-TA, the pseudo-first-order and pseudo-second-order models were employed and their linear plots are shown in Figures 6f and 6g, respectively. The kinetic parameters obtained from the above-mentioned kinetic models and the regression coefficients (R^2) are summarized in Table 1. The R^2 were very low, and the equilibrium adsorption capacities calculated from the pseudo first-order model were not fit well with the experimental data. In contrast, the values of R^2 , as well as the closeness of experimental and theoretical adsorption capacity (q_e) value showed the applicability of the second order model to describe the experimental data, with the determined values of 0.999. Furthermore, there is a good match between q_e values calculated from the pseudo-second-order model and q_e experimental results. Therefore, the mechanism concerning adsorption of MB on PAN-TA can be better explained by pseudo-second-order reaction kinetics.

Moreover, the intra-particle diffusion model was used to investigate the diffusion mechanism of MB molecules on PAN-TA. The curves of intra-particle diffusion model (Figure 6h) displayed three linear stages during the adsorption process. The first stage represented the diffusion of MB molecules from aqueous solution to the external surface of PAN-TA nanofibers, and the second stage represented the intra-particle diffusion of MB molecules from the external surface of PAN-TA to its internal surface.

Table 1. Pseudo-first-order, pseudo-second-order and intra-particle diffusion kinetic model parameters

$C_0 / (\text{mg L}^{-1})$	Pseudo-first-order kinetics				Pseudo-second-order kinetics			Intra-particle diffusion model			
	$q_{e,\text{exp}} / (\text{mg g}^{-1})$	$q_{e,\text{cal}} / (\text{mg g}^{-1})$	k_1 / min^{-1}	R^2	$q_{e,\text{cal}} / (\text{mg g}^{-1})$	$k_2 / (\text{g mg}^{-1} \text{min}^{-1})$	R^2	k_1	k_2	k_3	R^2
5	4.89	0.43	0.0138	0.6231	4.91	0.1662	0.9993	4.21	0.65	0.0021	0.9991
10	9.55	0.82	0.0093	0.6826	9.54	0.0689	0.9989	8.73	1.76	-0.0024	0.9923
20	18.49	5.06	0.0109	0.7219	18.46	0.0105	0.9983	13.49	24.90	-0.0069	0.9936

C_0 : initial concentration of dye; $q_{e,\text{exp}}$, $q_{e,\text{cal}}$: experimental and calculated MB adsorption capacity at equilibrium, respectively; k_1 , k_2 , k_3 : rate constants; R^2 : regression coefficient.

Moreover, intra-particle diffusion rate constants in every step follow the order of $k_1 > k_2 > k_3$, implying that the intra-particle diffusion was not just the rate-limiting step, both the film diffusion and intra-particle diffusion controlled the adsorption process. In addition, it was clear that the third stage of the curve was nearly parallel, which suggested that the equilibrium state reached at last.

Adsorption isotherms of MB adsorption onto PAN-TA

The parameters obtained from the experimental data using the isotherm and the related correlation coefficients are presented in Table 2 and Figure 7. Compared to Freundlich and Temkin model, the Langmuir model employed to describe the adsorption process fits better due to the higher value of R^2 , indicating the monolayer

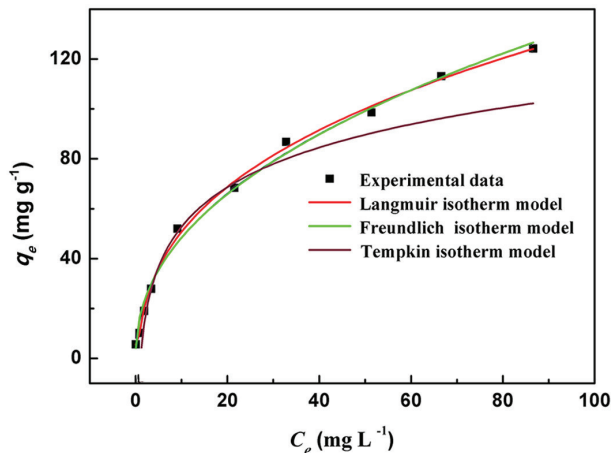


Figure 7. Non-linear Langmuir, Freundlich and Temkin isotherm for the adsorption of MB. Volume, 10 mL; adsorbent dose, 0.01 g; pH value, 8.0; contact time, 150 min; temperature, 25 °C; rotating speed, 150 rpm.

Table 2. Parameters of different isotherms for adsorption of MB on PAN-TA

Langmuir			Freundlich			Temkin			
$q_L / (\text{mg g}^{-1})$	$k_L / (\text{L mg}^{-1})$	R^2	$k_f / (\text{L mg}^{-1})$	$n / (\text{L mg}^{-1})$	R^2	$k_T / (\text{mg L}^{-1})$	$\beta / (\text{L mg}^{-1})$	$b / (\text{J mol}^{-1})$	R^2
155.4	0.612	0.9946	18.26	2.46	0.9812	1.31×10^4	10.21	141.16	0.8612

q_L : maximum MB adsorption capacity of PAN-TA; k_L : constant related to the rate of adsorption; R^2 : regression coefficient; k_f : extent of attraction; n : inverse of strength of attraction; k_T : constant of the Temkin isotherm; β : heat of adsorption; b : energy constant.

coverage of MB onto adsorbent. The maximum adsorption of PAN-TA for MB obeys Langmuir isotherm model. The adsorption capacities based on the Langmuir isotherm is 155.4 mg g^{-1} at 25 °C. Table 3 shows a comparison of q_L values related to different sorbents obtained by other researchers. Although q_L values of PAN-TA is not the highest, the advantages of our system compared to more adsorptive ones found in literature were as follows: on one hand, polyacrylonitrile yarn waste in the textile industry is always abandoned, which is a huge waste. It may be used as a raw material for the production of nanofibers by electrospinning. On the other hand, the nanofibrous composite adsorbents produced by the electrospinning technique are simple treatment methods along with other good features like large surface area, high porosity and good antimicrobial properties, forecasting a broad application prospects for MB removal from wastewater.

Antimicrobial performance

After 16 h, clear inhibition zones in a ring form around the PAN-TA nanofibers with a radius of 17.9 mm appeared in the Luria-Bertani (LB) agar plate (Figure 8). However, no inhibition zone was observed for the other plate (pure PAN). These results showed that the PAN-TA nanofibers exhibited better antimicrobial activities than the PAN nanofibers. It was essential that the silver nanoparticles which possessed effective sterilization, were incorporated into the PAN-TA nanofibers to make it powerful antibacterial. The mechanism why the PAN-TA nanofibers had antimicrobial activities could be explained. It is reported that Ag_3VO_4 nanoparticles could bind to the deoxyribonucleic acid (DNA) of the microorganisms, and

Table 3. Comparison of maximum adsorption capacity of MB onto various adsorbents

Adsorbent	$q_L / (\text{mg g}^{-1})$	Recycling / cost	Antimicrobial	Reference
Freeze-dried agarose gel	10.40	easy / expensive	no	42
Defatted algal biomass	7.73	easy / expensive	no	43
Activated carbon	70.92	easy / inexpensive	no	44
Calcium dodecyl sulfate enhanced precipitation	49.32	difficult / inexpensive	no	45
Naturally abundant zeolite	27.20	difficult / inexpensive	no	46
Sericin / β -cyclodextrin / PVA nanofiber ^a	187.97	difficult / expensive	no	47
Poly(methyl methacrylate) nanofiber	10.84	difficult / expensive	no	48
Mixed oxide nanoparticles	162.96	easy / expensive	no	32
Cellulose / graphene oxide	480.77	easy / expensive	no	49
CNTs-CoFe ₂ O ₄ @PPy ^b	137.00	easy / expensive	no	50
Starch functionalized magnetic MWCNT ^c	94	difficult / expensive	no	51
Polymer modified magnetic NPs ^d	129	difficult / inexpensive	no	52
PAN-TA ^e	155.40	easy / inexpensive	yes	this work

^aPVA: poly(vinyl alcohol); ^bpolypyrrole/CNTs-CoFe₂O₄ magnetic nanohybrid, CNT: carbon nanotube; ^cMWCNT: multi-walled carbon nanotube; ^dnanoparticles; ^epolyacrylonitrile-TiO₂-Ag₃VO₄.

then disturb their metabolism processes, especially cell division, which ultimately results in cell damage or death.²⁷ Moreover, Ag₃VO₄ could generate electron-pair holes and react with O₂ or OH⁻ to make active oxygen species formation, which interact with cell membranes, DNA, and cellular proteins, giving rise to cell death.⁵³

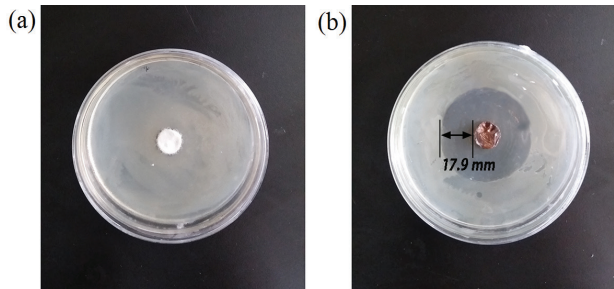


Figure 8. Photograph images of the zone of inhibition of (a) PAN and (b) PAN-TA composite nanofiber by the modified Kirby-Bauer test.

Photocatalytic removal of dyes under UV irradiation

Mixed metal oxides containing two or more metals

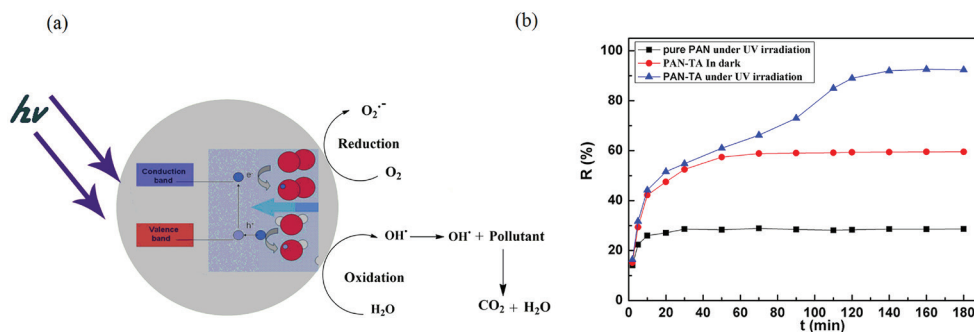


Figure 9. (a) Proposed mechanism of photocatalytic reaction on PAN-TA nanofibers; (b) removal rate of MB dyes by PAN-TA composite nanofibers under different experimental conditions.

have been shown to be effective catalysts and catalytic supports for a wide variety of organic reactions. TiO₂ and Ag₃VO₄ have been widely utilized to eliminate or degrade several organic dyes through radical mediated oxidation processes because of their good photocatalytic performance. Figure 9a shows the proposed mechanism of photocatalytic reaction. Then the photocatalytic performance of the PAN-TA composite nanofiber was evaluated by photodegradation of MB under UV irradiation (365 nm, 300 W) and monitored by determining the decrease in absorbance by UV-Vis spectrophotometry. In this study, the pure PAN nanofibers (0.01 g) and the mixture of PAN-TA composite nanofibers (0.01 g) were added to 25 mL of MB solution (50 mg L⁻¹), respectively. Then they were illuminated with UV lamp. The investigation of the photocatalytic activity of the nanoparticles was described in Figure 9b. For nanofibers without any inorganic particles (pure PAN) under UV irradiation (365 nm, 300 W), the concentration of MB has no significant change, as well as the removal efficiency (about 28.7%), indicating that MB molecules were

relatively stable and the self-photolysis process can be ignored. It was observed that the removal rate of MB dye under UV irradiation was higher than in dark. The degradation performance of the material for MB over the first 10 min was only 42.2%, then it increased to reach 92.48% when the reaction time was 3 h. Therefore, PAN-TA composite nanofiber has a promising application in the treatment of MB dye-containing effluents.

Regenerative performance

Recyclability is often seen as one of the important parameters for evaluating the practical application of adsorbent. In this work, we carried out the adsorption and desorption experiments in order to study the recyclability of prepared PAN-TA nanofibers. Interestingly, under the same circumstances, PAN-TA nanofibers showed only 10.6% decrease in their removal efficiency after 6th cycle (Figure 10), compared with the first cycle (96.2%). These results indicated that the prepared adsorbent possess excellent regeneration ability toward removal of MB.

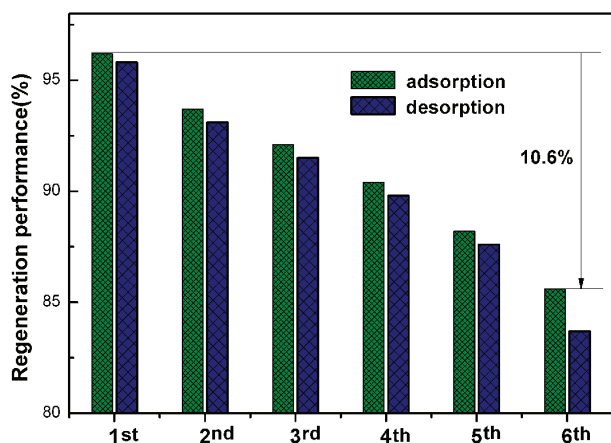


Figure 10. Regeneration tests for the MB adsorption onto PAN-TA by using HCl. Initial dyes concentration, 5 mg L⁻¹; adsorption pH: 8.0 (MB); temperature, 25 °C.

Conclusions

In this paper, a novel electrospun nanofibrous composite embedded with well-dispersed Ti, Ag nanoparticles was proposed in the present study and exhibited excellent adsorption performance for MB. The pH of the solution, temperature, contact time, dosage, initial dye concentration and chemical modification have significant impact on the adsorption process and capacity. Kinetics and adsorption equilibrium isotherms were investigated to help understand the adsorption properties of PAN-TA composite nanofibers. The adsorption data showed that it fitted well with the pseudo-second-order model and the maximum adsorption

capacity is 155.4 mg g⁻¹ at 25 °C calculated by Langmuir isotherm model. From a practical point of view, the nanofibrous composite adsorbent could be easily separated from the dye solution and displayed good reuse properties. Consequently, PAN-TA composite nanofiber mat may be used as a promising adsorbent for removal of dye from wastewater.

Acknowledgments

This work was supported by the Doctoral Scientific Research Foundation of Fuzhou University (No. 022578).

References

- Kolbasov, A.; Sinha-Ray, S.; Yarin, A. L.; Pourdeyehimi, B.; *J. Membr. Sci.* **2017**, *530*, 250.
- Wawrzekiewicz, M.; Bartczak, P.; Jesionowski, T.; *Int. J. Biol. Macromol.* **2017**, *99*, 754.
- Rahimdokht, M.; Pajootan, E.; Arami, M.; *Desalin. Water Treat.* **2016**, *57*, 18049.
- Agarwal, S.; Sadegh, H.; Monajjemi, M.; Hamdy, A. S.; Ali, G. A. M.; Memar, A. O. H.; Shahryari-ghoshekandi, R.; Tyagi, I.; Gupta, V. K.; *J. Mol. Liq.* **2016**, *218*, 191.
- Gonzalez, J. A.; Villanueva, M. E.; Piehl, L. L.; Copello, G. J.; *Chem. Eng. J.* **2015**, *280*, 41.
- Zahrim, A. Y.; Tizaoui, C.; Hilal, N.; *Desalination* **2011**, *266*, 1.
- Robati, D.; Mirza, B.; Ghazisaeidi, R.; Rajabi, M.; Moradi, O.; Tyagi, I.; Agarwal, S.; Gupta, V. K.; *J. Mol. Liq.* **2016**, *216*, 830.
- Kumar, K. V.; Ramamurthi, V.; Sivanesan, S.; *J. Colloid Interface Sci.* **2005**, *284*, 14.
- Vadivelan, V.; Kumar, K. V.; *J. Colloid Interface Sci.* **2005**, *286*, 90.
- Dutta, K.; Mukhopadhyay, S.; Bhattacharjee, S.; Chaudhuri, B.; *J. Hazard. Mater.* **2001**, *84*, 57.
- Li, Q.; Li, Y.; Ma, X.; Du, Q.; Sui, K.; Wang, D.; Wang, C.; Li, H.; Xia, Y.; *Chem. Eng. J.* **2017**, *316*, 623.
- Qi, Y.; Yang, M.; Xu, W.; He, S.; Men, Y.; *J. Colloid Interface Sci.* **2017**, *486*, 84.
- Ting, H.-F.; Chen, C.-M.; Lu, F.-H.; Suen, S.-Y.; *J. Taiwan Inst. Chem. Eng.* **2014**, *45*, 617.
- Almasian, A.; Mahmoodi, N. M.; Olya, M. E.; *J. Ind. Eng. Chem.* **2015**, *32*, 85.
- Jung, K.-W.; Choi, B. H.; Hwang, M.-J.; Jeong, T.-U.; Ahn, K.-H.; *Bioresour. Technol.* **2016**, *219*, 185.
- Ahmad, A.; Rafatullah, M.; Sulaiman, O.; Ibrahim, M. H.; Hashim, R.; *J. Hazard. Mater.* **2009**, *170*, 357.
- Dogan, M.; Alkan, M.; Onganer, Y.; *Water, Air, Soil Pollut.* **2000**, *120*, 229.

18. Chandane, V.; Singh, V. K.; *Desalin. Water Treat.* **2016**, *57*, 4122.
19. Krishnan, K. A.; Ajmal, K.; Faisal, A. K.; Liji, T. M.; *Sep. Sci. Technol.* **2015**, *50*, 1147.
20. Cheng, M.; Zeng, G.; Huang, D.; Lai, C.; Wei, Z.; Li, N.; Xu, P.; Zhang, C.; Zhu, Y.; He, X.; *Appl. Microbiol. Biotechnol.* **2015**, *99*, 5247.
21. Yang, H.; Feng, Q.; *Microporous Mesoporous Mater.* **2010**, *135*, 124.
22. Marrakchi, F.; Ahmed, M. J.; Khanday, W. A.; Asif, M.; Hameed, B. H.; *Int. J. Biol. Macromol.* **2017**, *98*, 233.
23. Swaminathan, S.; Muthumanickam, A.; Imayathamizhan, N. M.; *Int. J. Environ. Sci. Technol.* **2015**, *12*, 3499.
24. Abu-Saied, M. A.; Abdel-Halim, E. S.; Fouda, M. M. G.; Al-Deyab, S. S.; *Int. J. Electrochem. Sci.* **2013**, *8*, 5121.
25. Almasian, A.; Fard, G. C.; Gashti, M. P.; Mirjalili, M.; Shourijeh, Z. M.; *Desalin. Water Treat.* **2016**, *57*, 10333.
26. Almasian, A.; Olya, M. E.; Mahmoodi, N. M.; *Fibers Polym.* **2015**, *16*, 1925.
27. Saud, P. S.; Ghouri, Z. K.; Pant, B.; An, T.; Lee, J. H.; Park, M.; Kim, H.-Y.; *Carbon Lett.* **2016**, *18*, 30.
28. Gawande, M. B.; Pandey, R. K.; Jayaram, R. V.; *Catal. Sci. Technol.* **2012**, *2*, 1113.
29. Sajjadi, A.; Ravandi, S. A. H.; Izadan, H.; Kadivar, N.; *J. Eng. Fibers Fabr.* **2016**, *11*, 43.
30. Guo, N.; Liang, Y.; Lan, S.; Liu, L.; Ji, G.; Gan, S.; Zou, H.; Xu, X.; *Appl. Surf. Sci.* **2014**, *305*, 562.
31. Zhou, J.; Hao, B.; Wang, L.; Ma, J.; Cheng, W.; *Sep. Purif. Technol.* **2017**, *176*, 193.
32. Pal, U.; Sandoval, A.; Madrid, S. I. U.; Corro, G.; Sharma, V.; Mohanty, P.; *Chemosphere* **2016**, *163*, 142.
33. Song, J.; Kang, H.; Lee, C.; Hwang, S. H.; Jang, J.; *ACS Appl. Mater. Interfaces* **2012**, *4*, 460.
34. Teixeira, R. S. P.; Correa, R. J.; Bello Forero, J. S.; Silva, M. G. S.; Oliveira, R. C. S.; Souza, R. S.; *J. Appl. Polym. Sci.* **2017**, *134*, 1.
35. Kumar, M.; Tripathi, B. P.; Shahi, V. K.; *J. Hazard. Mater.* **2009**, *172*, 1041.
36. Anwar, J.; Shafique, U.; Zaman, W.-uz; Salman, M.; Dar, A.; Anwar, S.; *Bioresour. Technol.* **2010**, *101*, 1752.
37. Jia, Z.; Li, Z.; Ni, T.; Li, S.; *J. Mol. Liq.* **2017**, *229*, 285.
38. Simonin, J.-P.; *Chem. Eng. J.* **2016**, *300*, 254.
39. Wang, Y.; Hu, L.; Zhang, G.; Yan, T.; Yan, L.; Wei, Q.; Du, B.; *J. Colloid Interface Sci.* **2017**, *494*, 380.
40. Ma, X.; Xue, L.; Li, X.; Yang, M.; Yan, Y.; *Ceram. Interfaces* **2015**, *41*, 11927.
41. Pourjavadi, A.; Nazari, M.; Kabiri, B.; Hosseini, S. H.; Bennett, C.; *RSC Adv.* **2016**, *6*, 10430.
42. Ghaedi, M.; Ghaedi, A. M.; Abdi, F.; Roosta, M.; Vafaei, A.; Asghari, A.; *Ecotoxicol. Environ. Saf.* **2013**, *96*, 110.
43. Chandra, T. S.; Mudliar, S. N.; Vidyashankar, S.; Mukherji, S.; Sarada, R.; Krishnamurthi, K.; Chauhan, V. S.; *Bioresour. Technol.* **2015**, *184*, 395.
44. Hameed, B. H.; Mahmoud, D. K.; Ahmad, A. L.; *J. Hazard. Mater.* **2008**, *158*, 65.
45. Yang, Z.; Li, M.; Yu, M.; Huang, J.; Xu, H.; Zhou, Y.; Song, P.; Xu, R.; *Chem. Eng. J.* **2016**, *303*, 1.
46. Aysan, H.; Edeballi, S.; Ozdemir, C.; Karakaya, M. C.; Karakaya, N.; *Microporous Mesoporous Mater.* **2016**, *235*, 78.
47. Zhao, R.; Wang, Y.; Li, X.; Sun, B. L.; Jiang, Z. Q.; Wang, C.; *Colloids Surf., B* **2015**, *136*, 375.
48. Koysuren, O.; Koysuren, H. N.; *J. Macromol. Sci., Part A* **2016**, *53*, 691.
49. Chen, L.; Li, Y.; Hu, S.; Sun, J.; Du, Q.; Yang, X.; Ji, Q.; Wang, Z.; Wang, D.; Xia, Y.; *J. Exp. Nanosci.* **2016**, *11*, 1156.
50. Li, X.; Lu, H.; Zhang, Y.; He, F.; *Chem. Eng. J.* **2017**, *316*, 893.
51. Chang, P. R.; Zheng, P.; Liu, B.; Anderson, D. P.; Yu, J.; Ma, X.; *J. Hazard. Mater.* **2011**, *186*, 2144.
52. Ge, F.; Ye, H.; Li, M.-M.; Zhao, B.-X.; *Chem. Eng. J.* **2012**, *198*, 11.
53. Vu, T. A.; Dao, C. D.; Hoang, T. T. T.; Dang, P. T.; Tran, H. T. K.; Nguyen, K. T.; Le, G. H.; Nguyen, T. V.; Lee, G. D.; *Mater. Lett.* **2014**, *123*, 176.

Submitted: June 6, 2017

Published online: September 22, 2017